Original research

Association of Glutamate and N-Acetylaspartate Levels with Abnormal Protein Deposition in Alzheimer's Disease: Insights from Magnetic Resonance Spectroscopic Imaging

Kiwamu Matsuoka [1, 2], Kosei Hirata [1], Naomi Kokubo [1], Takamasa Maeda [3], Kenji Tagai [1], Hironobu Endo [1], Keisuke Takahata [1], Hitoshi Shinotoh [1, 4], Maiko Ono [1,5], Chie Seki [1], Harutsugu Tatebe [1], Kazunori Kawamura [6], Ming-Rong Zhang [6], Hitoshi Shimada [1, 7], Takahiko Tokuda [1], Makoto Higuchi [1], Yuhei Takado [1, 5]

1. Department of Functional Brain Imaging, Institute for Quantum Medical Science, Quantum Life and Medical Science Directorate, National Institutes for Quantum Science and Technology, Chiba, Japan
2. Department of Psychiatry, Nara Medical University, Nara, Japan
3. QST Hospital, Quantum Life and Medical Science Directorate, National Institutes for Quantum Science and Technology, Chiba, Japan
4. Neurology Clinic, Chiba, Chiba, Japan
5. Institute for Quantum Life Science, Quantum Life and Medical Science Directorate, National Institutes for Quantum Science and Technology, Chiba, Japan
6. Department of Advanced Nuclear Medicine Sciences, Institute for Quantum Medical Science, Quantum Life and Medical Science Directorate, National Institutes for Quantum Science and Technology, Chiba, Japan
7. Center for integrated human brain science, Brain Research Institute, Niigata University, Niigata, Japan

***Corresponding Authors**:
Kiwamu MATSUOKA, MD, PhD
Department of Functional Brain Imaging Research, Institute for Quantum Medical Science, National Institutes for Quantum Science and Technology (QST), 4-9-1 Anagawa, Inage-ku, Chiba-shi, Chiba 263-8555, Japan
Tel. +81-43-206-3251 Fax: +81-43-253-0396
E-mail: matsuoka.kiwamu@qst.go.jp

Yuhei TAKADO, MD, PhD
Institute for Quantum Life Science, National Institutes for Quantum Science and

Technology (QST), 4-9-1 Anagawa, Inage-ku, Chiba-shi, Chiba 263-8555, Japan
Tel. +81-43-206-3183 Fax: +81-43-206-4191
E-mail: takado.yuhei@qst.go.jp

ABSTRACT

Background Accumulating evidence indicated decreased levels of glutamate (Glu) and N-acetylaspartate (NAA) in the posterior cingulate cortex (PCC) in Alzheimer's disease (AD) brains. However, the levels of these metabolites in the other brain regions and the associations with abnormal protein of AD remain to be elucidated.

Methods We enrolled 19 patients with AD and 26 healthy controls (HC). We performed magnetic resonance spectroscopic imaging (MRSI) to evaluate Glu/creatine (Cr) and NAA/Cr ratios and measure plasma neurofilament light chain (NfL) levels. We examined tau and amyloid-β depositions with standardized uptake value ratios (SUVRs) of florzolotau (18F) and ^{11}C-PiB positron emission tomography, respectively. Heatmaps were created to visualize Z scores of Glu/Cr and NAA/Cr ratios using HC data.

Results In the AD brains, Z-score maps demonstrated reduced Glu/Cr and NAA/Cr ratios in the gray matter, including the right dorsolateral prefrontal cortex (DLPFC) and PCC; Glu/Cr ratios negatively correlated with florzolotau (18F) SUVRs in the PCC; mini-mental state examination total scores correlated with Glu/Cr ($P < 0.001$, $r = 0.72$) and NAA/Cr ratios ($P < 0.001$, $r = 0.75$) in the right DLPFC; and blood NfL levels were increased and negatively correlated with the Glu/Cr ($P = 0.040$, $r = -0.50$) and NAA/Cr ratios ($P = 0.003$, $r = -0.68$) in the right DLPFC.

Conclusions Our findings indicated that decreased Glu/Cr levels correlated with tau pathologies of AD in the PCC. MRSI is capable of providing spatial information on neural function, enabling the identification of vulnerabilities in the right DLPFC in AD pathology.

INTRODUCTION

Alzheimer's disease (AD) is a progressive neurodegenerative disease often characterized by initial memory impairment following a cognitive decline [1]. A recent study reported the prevalence of clinical AD in the United States to be 11.3% and predicted further increases in the next four decades [2]. AD is a very burdensome disease, ranking fourth-highest in years of life lost in 2016 [3]. The neuropathologic hallmark of AD is neuronal loss paralleled by the distribution of neurofibrillary tangles composed of filamentous tau proteins and amyloid plaques [4]. The limited cognitive improvement observed upon removal of amyloid plaques with human monoclonal antibodies [5] suggests that therapeutic approaches that address other factors, including abnormal tau protein and neuronal dysfunction, may be necessary. To develop disease-modifying treatments based on the underlying pathophysiology, it is essential to investigate the relationship between tau protein and neuronal dysfunction *in vivo*. However, to the best of our knowledge, only a small number of studies have investigated this relationship [6].

Proton magnetic resonance spectroscopy (MRS) can potentially inform us about neuronal dysfunction in diseased brains using two major metabolites, N-acetylaspartate (NAA) and glutamate (Glu). While NAA has been employed as a primary neuronal marker of viability [7], Glu measured by MRS could be a marker of metabolic activity [7] in the brain due to its relationship with glucose metabolism [8]. A recent meta-analysis of patients with AD revealed reduced Glu levels in the posterior cingulate cortex (PCC) accompanied by reduced NAA levels [9]. It is speculated that Glu may be an important metabolite in AD with a potential association with tau proteins; however, it has not been examined outside of the PCC using MRS, and the mechanism by which its relationship to abnormal proteins differs from NAA is not fully understood. This non-invasive modality can be combined with other modalities, such as positron emission tomography (PET) to evaluate brain conditions from multiple aspects.

The advent of PET has enabled the evaluation of tau and amyloid-β deposition in AD pathology [10]. We reported that florzolotau (18F) (^{18}F-florzolotau) could visualize tau depositions with high contrast in patients with AD [11]. A recent study showed that tau aggregations were associated with neuronal dysfunction evaluated by NAA and Glu levels in the PCC in cognitively unimpaired older adults [6]. In the previous study, individuals with only slight abnormal protein accumulations were not excluded due to an absence cutoff of the PET standardized uptake value ratio (SUVR). On the other hand, to our knowledge, no *in vivo* imaging studies investigated the associations of NAA and Glu levels with tau aggregations in patients who developed

AD.

In this study, we utilized MRS imaging (MRSI) of the cingulate gyrus of patients with AD to assess the levels of NAA and Glu, which are indicative of neuronal viability and metabolic activity, respectively. In addition, we explored the connection between these MRSI measurements and the distribution of abnormal proteins measured by PET to elucidate their relationship. Moreover, we evaluated the clinical utility of MRS metabolites by examining the association between the blood levels of neurofilament light chain (NfL), which provides a sensitive measurement of neuroaxonal damage, and the MRS metabolites (Glu and NAA).

MATERIALS AND METHODS

Participants

We recruited patients with mild cognitive impairment (MCI) due to AD and AD dementia from affiliated hospitals of the National Institute of Radiological Sciences (NIRS) and National Institutes for Quantum Science and Technology (QST) between April 2019 and September 2021. All the patients with MCI due to AD and AD dementia were diagnosed using the criteria for MCI defined by Petersen [12] and the NINCDS-ADRDA Alzheimer's Criteria as probable AD [13], respectively. We also recruited age- and sex-matched healthy controls (HCs) from the volunteer association of the NIRS-QST. All the HCs had no history of neurologic or psychiatric disorders. At the screening, all the patients with AD and HCs were confirmed to be with and without amyloid deposition, respectively, by visual assessment of PET images of ^{11}C-Pittsburgh compound-B (PiB) by three readers based on the standard method used in the Japanese Alzheimer's Disease Neuroimaging Initiative (J-ADNI) study [14]. We excluded one patient with AD and one HC because they did not complete the imaging protocol. Thirteen patients were exposed to cholinesterase inhibitors for AD (donepezil, n = 10; galantamine, n = 1; rivastigmine, n = 2). Meanwhile, we excluded one patient with AD who took memantine, a glutamate receptor antagonist. Finally, we enrolled 19 patients with AD and 27 HCs. We obtained written informed consent from all the participants and/or from spouses or other close family members when the patients were cognitively impaired. The QST Certified Review Board approved the current study.

All the participants were subjected to a series of standardized quantitative measurements of cognitive function (Mini-Mental State Examination [MMSE] [15] and Clinical Dementia Rating [CDR] [16] for patients with AD) and neuropsychiatric symptoms (Apathy scale [17] and Geriatric Depression Scale [GDS] [18]). All the HCs and some patients with AD completed the Trail Making Test [TMT] [19] (18 patients for TMT-A and 15 patients for TMT-B).

MRI / MRSI data acquisition and analysis

MRI and MRSI scans were performed using a 3.0-Tesla scanner (MAGNETOM Verio; Siemens Healthcare) equipped with a 32-channel receiving head coil. Three-dimensional T1-weighted images were acquired using a magnetization-prepared rapid gradient-echo sequence (repetition time (TR) = 2,300 ms; echo time (TE) = 1.95 ms; TI = 900 ms; field of view (FOV) = 250 mm; flip angle = 9°; acquisition matrix = 256 × 256; and axial slices of 1 mm thickness). We also performed a two-dimensional MRSI with point-resolved spectroscopy (PRESS) pulse sequence with the following

parameters: TE = 30 ms, TR = 2000 ms, 3 averages, 16 × 16 chemical shift imaging matrix, and slice thickness = 15 mm. Every single volume of interest (VOI) was 10 × 10 × 15 mm^3 (FOV = 160 × 160 mm^2 including the measurement volume [mVol] = 80 × 80 × 15 mm^3). We applied 3D Shim (Syngo MR version for VD13A, Siemens, Erlangen, Germany) and subsequently performed manual shimming to reduce the linewidth of the water spectrum in magnitude mode below 25 Hz. Outer-volume suppression (OVS) [20] and water suppression were enhanced through T1 effects (WET) [21]. A trained operator placed the multi-voxel VOIs at the level of the cingulate gyrus (Figure 1).

PET procedures

All the participants were examined using ^{11}C-PiB and ^{18}F-florzolotau PET. ^{11}C-PiB and ^{18}F-florzolotau were radiosynthesized by the Department of Radiopharmaceuticals Development at NIRS following our previous studies' protocols [11, 22]. The ^{18}F-florzolotau (injected dose: 185.7 ± 6.9 MBq, molar activity: 248.6 ± 76.3 GBq/μmol) PET scan was performed using Biograph mCT flow system (Siemens Healthcare). The images were reconstructed with filtered back projection. Meanwhile, the ^{11}C-PiB (injected dose: 536.1 ± 61.1 MBq, molar activity: 87.2 ± 24.6 GBq/μmol) PET scan was performed using ECAT EXACT HR+ scanner (CTI PET Systems, Inc.), Biograph mCT flow system (Siemens Healthcare), or Discovery MI (GE Healthcare). All the PET scan images were reconstructed with filtered back projection.

MRSI data analysis

We analyzed MRSI data using LCModel software (Stephen Provencher, Inc) [23] for a linear combination of model spectra provided in a basis set. We evaluated the referencing metabolite ratios of total NAA (tNAA; NAA + N–acetyl–aspartyl–glutamate [NAAG]) and Glu to total creatine (Cr) (tCr; Cr + PCr), because tCr has been widely used as an internal reference in human studies [24]. The signal-to-noise ratio (SNR) was obtained using an NAA peak height at 2.01 ppm divided by the standard deviation (SD) of noise. For all spectra, LCModel quantification was performed on a spectral window between 0.2 and 4.2 ppm. We excluded spectra data of the most dorsal 8 voxels, based on the quality control criteria (SNR ratio < 5, full width at half maximum [FWHM] > 0.143 ppm) [25]. Additionally, data from one HC were excluded because of strong lipid contamination.

PET image processing

We applied motion correction and coregistration to the corresponding participant's

T1-weighted images for PET data using PMOD® software ver. 3.8 (PMOD Technologies Ltd., Zurich, Switzerland). SUVR images were generated with cerebellar gray matter (GM) as a reference region, using ^{18}F-florzolotau PET data at 90–110-min post-injection and ^{11}C-PiB PET data at 50–70 min post-injection. For the reference region, we performed surface-based cortical reconstruction and volumetric subcortical segmentation of T1-weighted images with FreeSurfer software (version 6.0.0; http://surfer.nmr.harvard.edu). We defined regions of interest (ROIs) of the cerebellar cortex [26] (excluding the vermis [27]) as described in our previous study [28].

We defined target ROIs corresponding to the multi-voxel VOIs of the measurement volume by MRSI. The multi-voxel VOIs were composed 8 × 8 voxels of 80 × 80 × 15 mm^3. We manually performed coregistration of the multi-voxel VOIs to the corresponding participant's T1-weighted images using screenshot images of the MRSI VOI placements as a reference (supplemental figure 1). We evaluated ^{18}F-florzolotau and ^{11}C-PiB SUVRs in the multi-voxel VOIs.

Immunoassay protocols

We measured plasma levels of the NfL from the blood samples of 26 HCs and 17 patients with AD. We applied an HD-X Simoa analyzer with reagents from a single lot using the Simoa NF-light assay, according to the protocol issued by the manufacturer (Quanterix, Lexington, MA, USA). All samples were analyzed in duplicate on one occasion.

Statistical analysis

Independent samples t-tests and χ^2-tests were used to compare baseline demographics, clinical characteristics, metabolite levels, NfL levels, and ^{18}F-florzolotau and ^{11}C-PiB SUVRs. Pearson correlation or Spearman's rank-order correlation was used to evaluate the correlations between clinical characteristics, metabolite levels, NfL levels, and ^{18}F-florzolotau and ^{11}C-PiB SUVRs. All statistical tests were two-tailed, and P values of <0.05 indicated statistical significance. Statistical analyses were performed using IBM SPSS Statistics for Windows, version 25 (IBM Corp., Armonk, NY, USA).

We constructed heatmaps to visualize Z scores of ^{18}F-florzolotau and ^{11}C-PiB SUVRs and the metabolites to tCr ratios in patients with AD using data of HCs as a reference. In addition, we created a heatmap of Pearson correlation coefficients between the metabolites to tCr ratios and SUVRs of ^{18}F-florzolotau and ^{11}C-PiB SUVRs in patients with AD. We utilized GraphPad Prism version 8.4.3 (GraphPad Software) for heatmaps. Based on the results of the heatmaps, we chose VOI for further analysis to

compare the metabolites with tCr ratios between patients with AD and HCs and the correlations with cognitive functions, NfL levels, and ^{18}F-florzolotau and ^{11}C-PiB SUVRs.

RESULTS

Demographic and clinical profiles

The demographic and clinical profiles of patients with AD and HCs are summarized in Table 1. The study included eight patients with MCI and 11 with dementia. There were no statistically significant differences in age or sex between the two groups. The patients with AD showed worse cognitive functions in the total scores of MMSE and TMT-A and TMT-B than those of the HCs. There were no statistically significant differences in the symptoms of depression (GDS) or apathy (AS) between the two groups.

Heatmaps of the Z score means of ^{18}F-florzolotau and ^{11}C-PiB SUVRs

All the patients with AD demonstrated typical depositions of ^{18}F-florzolotau in the neocortical and limbic cortices, in line with our previous study [11] (Figure 2a). They also showed ^{11}C-PiB depositions in the cortices corresponding to the J-ADNI study criteria [14] (Figure 2b). The heatmaps of the Z score means of ^{18}F-florzolotau and ^{11}C-PiB SUVRs were markedly increased in the neocortical and limbic cortices (Figure 2c, d).

Heatmaps of Glu/tCr and tNAA/tCr ratios

The heatmap showed decreased Z scores of Glu/tCr ratios in the GM, especially in the PCC and right dorsolateral prefrontal cortex (DLPFC) (Figure 3a). The heatmap also demonstrated decreases in tNAA/tCr ratios in the GM, including the PCC and right DLPFC (Figure 3b).

The heatmaps of Pearson correlation coefficients of ^{18}F-florzolotau and ^{11}C-PiB SUVRs showed a marked negative correlation of Glu/tCr ratios with ^{18}F-florzolotau SUVR in the PCC regions (Figure 3c-f).

Glu/tCr and tNAA/tCr ratios in the PCC and right DLPFC

Subsequently, we analyzed the combined voxels covering the PCC and right DLPFC (Figure 4a). We found that Glu/tCr and tNAA/tCr ratios were both significantly decreased in the PCC and right DLPFC in patients with AD compared with that of the HCs (Glu/tCr ratios, $P < 0.05$ in the PCC and $P < 0.005$ in the right DLPFC; tNAA/tCr ratios, $P < 0.05$ in the PCC and $P < 0.001$ in the right DLPFC) (Figure 4b-e). We also found a correlation between tNAA/tCr ratios in the PCC and right DLPFC ($r = 0.52$, $P = 0.023$), but not with Glu/tCr ($r = 0.16$, $P = 0.51$).

The heatmap revealed a negative correlation of SUVRs of ^{18}F-florzolotau

Glu/tCr ratios in the PCC but with not tNAA (Glu/tCr ratios, P = 0.046 and r = −0.46; tNAA/tCr ratios, P = 0.62 and r = 0.12) (Figure 5). There was no significant correlation with ^{11}C-PiB SUVRs in the PCC (Glu/tCr ratios, P = 0.53 and r = −0.15; tNAA/tCr ratios, P = 0.11 and r = 0.38). We observed no significant correlation with SUVRs of ^{18}F-florzolotau and ^{11}C-PiB in the right DLPFC (Glu/tCr ratios, P = 0.64 and r = −0.12; tNAA/tCr ratios, P = 0.19 and r = −0.32 for ^{18}F-florzolotau; Glu/tCr ratios, P = 0.46 and r = −0.18; tNAA/tCr ratios, P = 0.17 and r = −0.33 for ^{11}C-PiB).

In the right DLPFC, Glu/tCr and tNAA/tCr ratios were positively correlated with the MMSE total scores in patients with AD (Glu/tCr ratios, P < 0.001 and r = 0.72; tNAA/tCr ratios, P < 0.001 and r = 0.75) (Figure 6a, b); the Glu/tCr and tNAA/tCr ratios were not correlated in the PCC (Glu/tCr ratios, P = 0.15 and r = 0.35; tNAA/tCr ratios, P = 0.14 and r = 0.35). In patients with AD, we also found negative correlations between Glu/tCr ratios in the PCC and TMT-A time and between tNAA/tCr ratios in the right DLPFC and TMT-B time (Glu/tCr ratios, P = 0.002 and r = −0.68; tNAA/tCr ratios, P = 0.53 and r = −0.16 in the PCC; Glu/tCr ratios, P = 0.22 and r = −0.31; tNAA/tCr ratios, P = 0.050 and r = −0.47 in the right DLPFC for TMT-A; Glu/tCr ratios, P = 0.83 and r = −0.061; tNAA/tCr ratios, P = 0.55 and r = 0.17 in the PCC; Glu/tCr ratios, P = 0.95 and r = 0.017; tNAA/tCr ratios, P = 0.007 and r = −0.66 in the right DLPFC for TMT-B) (Figure 6c, d).

Correlations of Glu/tCr and tNAA/tCr ratios in the PCC and right DLPFC with blood NfL levels

We found higher NfL levels in the blood in patients with AD than that in the HCs (P < 0.005) (Figure 7a). We found negative correlations between blood NfL levels and Glu/tCr ratios (P = 0.040 and r = −0.50) and tNAA/tCr ratios (P = 0.003 and r = −0.68) in the right DLPFC. There were also trends of negative correlations between blood NfL levels and Glu/tCr ratios (P = 0.10 and r = −0.41) or tNAA/tCr ratios (P = 0.086 and r = −0.43) in the PCC, although these correlations did not reach a statistical significance level (Figure 7b-e).

DISCUSSION

The MRSI technique revealed decreases in Glu/tCr and tNAA/tCr ratios in the PCC and right DLPFC, which were associated with impaired cognitive functions in patients with AD. Glu/tCr ratios, rather than tNAA/tCr ratios, exhibited a negative correlation with the levels of tau depositions in the PCC. Moreover, Glu/tCr and tNAA/tCr ratios in the right DLPFC were negatively associated with NfL levels, which provide a sensitive measurement of neuroaxonal damage.

Decreased Glu levels associated with tau deposition levels in the PCC of AD brains

The Glu/tCr and tNAA/tCr ratios in the PCC were lower in patients with AD compared with that of the HCs. While only the Glu/tCr ratio was found to correlate with ^{18}F-florzolotau SUVRs in the PCC, the lack of correlation with the tNAA/tCr ratios requires further investigation. Glu is an essential metabolic biomarker, as previous research indicates that more than 50% of glucose eventually metabolizes to glutamate in the brain [8]. A recent meta-analysis study has linked reduced brain glucose metabolism, mitochondrial dysfunction, and oxidative stress to tau pathology in AD, which induces synaptic damage and neuronal death. In a previous study, the observed correlation between tau accumulation levels and Glu levels in the PCC of cognitively unimpaired subjects is consistent with our findings [6]. Future preclinical studies could use a tauopathy mouse model to investigate the role of impaired brain glucose metabolism and mitochondrial function to elucidate the underlying mechanism of the relationship between decreased Glu levels and tau depositions. Furthermore, longitudinal studies in human and tau mouse models may clarify the time series of these associations.

MRSI revealed decreased metabolic activities in the right DLPFC in patients with AD

In an exploratory MRSI study, reduced Glu/tCr and tNAA/tCr ratios were observed not only in the PCC but also in the right DLPFC, indicating the potential for the latter region to be a useful assessment region for MRS [29, 30]. Prior studies on Glu levels in the DLPFC of patients with AD have reported inconsistent results, potentially due to the evaluation of Glx (Glu + glutamine [Gln]) rather than Glu alone. However, our measurement of Glu levels independent from Gln levels revealed reduced Glu levels in the right DLPFC of patients with dementia due to MCI and AD. Differences in AD and HC were observed in the right DLPFC but not in the left dominant hemisphere. While this study only captured changes in the right DLPFC, the differences between the left and right DLPFC in patients with AD patients remain unclear. The results of a previous

study utilizing ^{18}F-FDG PET were in agreement with our investigations, indicating a decrease in metabolism of the DLPFC in the early stages of AD [31], particularly in the right hemisphere [32]. Nevertheless, MRSI is not without limitations, because chemical shift displacement may introduce ambiguity when interpreting interhemispheric discrepancies. Therefore, validation of the left–right difference of DLPFC function in AD should be further pursued using advanced MRS techniques, such as sLASER [33], which exhibits lower chemical shift displacement.

Conversely, our findings in the right DLPFC revealed positive associations between the Glu/tCr and tNAA/tCr ratios and the overall MMSE scores, while the tNAA/tCr ratio demonstrated an inverse correlation with TMT-B completion time. These results indicate that the outcomes in the right DLPFC are not a happenstance, but rather hold potential as a valuable appraisal domain for MRS, akin to the PCC. Given that the DLPFC has been shown to play a critical role in visual working memory [34, 35], it is plausible that reduced metabolic activity and neuronal survival in patients with AD may be linked to compromised working memory function.

MRSI and blood biomarkers revealed impaired neural functions in patients with AD

Both MRSI and blood biomarkers showed neural dysfunctions in patients with AD, and as an alternative to PET, blood biomarkers and MRSI measurements are less invasive and less costly, making them potentially appropriate for use in primary care. Blood biomarkers, in particular, require less testing time. NfL has been established as a biomarker of neural damage in various neurological diseases, including AD, based on accumulating evidence [36]. MRSI is a non-invasive technique that provides spatial information on metabolite levels in the brain without requiring additional imaging modalities. However, the practical application of MRSI may be limited by the technical expertise required for imaging and data analysis. In this study, a single-slice MRSI approach was used to cover a portion of the brain region of interest, but recent technological advancements have enabled 3D imaging. Although resting-state functional MRI has been extensively utilized to assess the functional network of brain diseases, MRSI can directly evaluate neural viability and metabolic activity, and thus may provide useful complementary information for future brain network assessment from a different perspective.

CONCLUSION

The MRSI technique revealed neural dysfunctions, including metabolic activity, linked

with tau aggregations in the PCC. MRSI has the potential to provide spatial information regarding neural functions, leading to our findings of deteriorated neural viability and metabolic activity in the right DLPFC of patients with AD. MRSI could qualify metabolic levels in several brain regions simultaneously. The robustness of MRSI data was demonstrated by its relationship with NfL, which is commonly used in blood biomarker studies. Together with resting-state functional MRI, these MRSI measurements may have the potential to elucidate brain network impairments.

ACKNOWLEDGMENTS

The authors thank all patients and their caregivers for participation in this study, clinical research coordinators, PET and MRI operators, animal care technicians, radiochemists, and research ethics advisers at QST for their assistance in the current projects. We thank APRINOIA Therapeutics for kindly sharing the precursor of ^{18}F-florzolotau. The authors acknowledge support for the recruitment of patients by Dr. Shigeki Hirano at the Chiba University and Dr. Yasumasa Yoshiyama, at Inage Neurology and Memory Clinic.

FUNDING

This study was also supported in part by AMED under grant numbers JP18dm0207018, JP19dm0207072, JP18dk0207026, JP19dk0207049, and 22dk0207063, and JSPS KAKENHI grant numbers JP19H01041, JP16H05324, JP18K07543, and JP20K16681.

DECLARATION OF COMPETING INTEREST

H.S. (Hitoshi Shimada), M.-R.Z., T.S., and M.H. hold patents on compounds related to the present report (JP 5422782/EP 12 884 742.3/CA2894994/HK1208672). All other authors report no biomedical financial interests or potential conflicts of interest.

CONTRIBUTORS

Conceived and designed the study: K.M., Y.T. Supervised the project: M.-R.Z., T.T., M.H. Performed scans and tests: K.M., K.H., N.K., T.M., K.T. (Kenji Tagai), H.E., K.T. (Keisuke Takahata), H.S. (Hitoshi Shinotoh), and K.K., H.S. (Hitoshi Shimada). Analyzed MRS data: K.M., K.H., T.M., Y.T. Analyzed PET data: K.M., K.H., K.T. (Kenji Tagai), H.E., C.S. Analyzed biomarker data: K.T. (Kenji Tagai), H.T., T.T., Performed statistical analysis: K.M., Y.T. Interpreted the data: K.M., K.H., N.K., T.M., K.T. (Kenji Tagai), H.E., K.T. (Keisuke Takahata), H.S. (Hitoshi Shinotoh), M.O., C.S., H.T., K.K., M.-R.Z., H.S. (Hitoshi Shimada), T.T., M.H., Y.T., Wrote the first draft: K.M., Y.T. Reviewed manuscript: K.M., K.H., N.K., T.M., K.T. (Kenji Tagai), H.E., K.T. (Keisuke Takahata), H.S. (Hitoshi Shinotoh), M.O., C.S., H.T., K.K., M.-R.Z., H.S. (Hitoshi Shimada), T.T., M.H., Y.T., K.M., and Y.T. are responsible for the overall content as a guarantor.

PATIENT CONSENT FOR PUBLICATION

Obtained.

ETHICS APPROVAL

This study was approved by the Institutional Review Board of the NIRS. Written informed consent was obtained from all patients and from their spouses or other close family members. The study was registered with the UMIN clinical Trials Registry (UMIN-CTR; number 000030248).

DATA AVAILABILITY STATEMENT

Data are available upon reasonable request. Anonymized raw data supporting the findings of the present study may be shared upon request with the corresponding author.

REFERENCES

1 Jack CR, Jr., Knopman DS, Jagust WJ, et al. Tracking pathophysiological processes in Alzheimer's disease: an updated hypothetical model of dynamic biomarkers. Lancet Neurol 2013;12:207–16. doi: 10.1016/S1474-4422(12)70291-0.

2 Rajan KB, Weuve J, Barnes LL, et al. Population estimate of people with clinical Alzheimer's disease and mild cognitive impairment in the United States (2020-2060). Alzheimers. Dement 2021;17:1966–75. doi: 10.1002/alz.12362.

3 US Burden of Disease Collaborators, Mokdad AH, Ballestros K, et al. The state of US health, 1990-2016: burden of diseases, injuries, and risk factors among US states. JAMA 2018;319:1444–72. doi: 10.1001/jama.2018.0158.

4 DeTure MA, Dickson DW. The neuropathological diagnosis of Alzheimer's disease. Mol Neurodegener 2019;14:32. doi: 10.1186/s13024-019-0333-5.

5 Sevigny J, Chiao P, Bussière T, et al. The antibody aducanumab reduces Aβ plaques in Alzheimer's disease. Nature 2016;537:50–6. doi: 10.1038/nature19323.

6 Kara F, Joers JM, Deelchand DK, et al. 1H MR spectroscopy biomarkers of neuronal and synaptic function are associated with tau deposition in cognitively unimpaired older adults. Neurobiol Aging 2022;112:16–26. doi: 10.1016/j.neurobiolaging.2021.12.010.

7 Rae CD. A guide to the metabolic pathways and function of metabolites observed in human brain 1H magnetic resonance spectra. Neurochem Res 2014;39:1–36. doi: 10.1007/s11064-013-1199-5.

8 Sugiura Y, Honda K, Kajimura M, et al. Visualization and quantification of cerebral metabolic fluxes of glucose in awake mice. Proteomics 2014;14:829–38. doi: 10.1002/pmic.201300047.

9 Liu H, Zhang D, Lin H, et al. Meta-analysis of neurochemical changes estimated via magnetic resonance spectroscopy in mild cognitive impairment and Alzheimer's disease. Front Aging Neurosci 2021;13:738971. doi: 10.3389/fnagi.2021.738971.

10 Maschio C, Ni R. Amyloid and tau positron emission tomography imaging in Alzheimer's disease and other tauopathies. Front Aging Neurosci 2022;14:838034. doi: 10.3389/fnagi.2022.838034.

11 Tagai K, Ono M, Kubota M, et al. High-contrast in vivo imaging of tau pathologies in Alzheimer's and non-Alzheimer's disease tauopathies. Neuron 2021;109:42–58.e8. doi: 10.1016/j.neuron.2020.09.042.

12 Petersen RC, Smith GE, Waring SC, et al. Mild cognitive impairment: clinical characterization and outcome. Arch Neurol 1999;56:303–8. doi: 10.1001/archneur.56.3.303.

13 McKhann G, Drachman D, Folstein M, et al. Clinical diagnosis of Alzheimer's disease: report of the NINCDS-ADRDA Work Group under the auspices of Department of Health and Human Services Task Force on Alzheimer's Disease. Neurology 1984;34:939–44. doi: 10.1212/wnl.34.7.939.

14 Yamane T, Ishii K, Sakata M, et al. Inter-rater variability of visual interpretation and comparison with quantitative evaluation of (11)C-PiB PET amyloid images of the Japanese Alzheimer's Disease Neuroimaging Initiative (J-ADNI) multicenter study. Eur J Nucl Med Mol Imaging 2017;44:850–57. doi: 10.1007/s00259-016-3591-2.

15 Folstein MF, Folstein SE, McHugh PR. "Mini-mental state". A practical method for grading the cognitive state of patients for the clinician. J Psychiatr Res 1975;12:189–98. doi: 10.1016/0022-3956(75)90026-6.

16 Morris JC. Clinical dementia rating: a reliable and valid diagnostic and staging measure for dementia of the Alzheimer type. Int Psychogeriatr 1997;9 (**Suppl. 1**):173–6. doi: 10.1017/s1041610297004870.

17 Starkstein SE, Fedoroff JP, Price TR, et al. Apathy following cerebrovascular lesions. Stroke 1993;24:1625–30. doi: 10.1161/01.str.24.11.1625.

18 Lesher EL, Berryhill JS. Validation of the geriatric depression scale--short form among inpatients. J Clin Psychol 1994;50:256–60. doi: 10.1002/1097-4679(199403)50:2<256::aid-jclp2270500218>3.0.co;2-e.

19 Tombaugh TN. Trail making test A and B: normative data stratified by age and education. Arch Clin Neuropsychol 2004;19:203–14. doi: 10.1016/S0887-6177(03)00039-8.

20 Tkác I, Andersen P, Adriany G, et al. In vivo 1H NMR spectroscopy of the human brain at 7 T. Magn Reson Med 2001;46:451–6. doi: 10.1002/mrm.1213.

21 Ogg RJ, Kingsley PB, Taylor JS. WET, a T1- and B1-insensitive water-suppression method for in vivo localized 1H NMR spectroscopy. J Magn Reson B 1994;104:1–10. doi: 10.1006/jmrb.1994.1048.

22 Maruyama M, Shimada H, Suhara T, et al. Imaging of tau pathology in a tauopathy mouse model and in Alzheimer patients compared to normal controls. Neuron 2013;79:1094–108. doi: 10.1016/j.neuron.2013.07.037.

23 Provencher SW. Estimation of metabolite concentrations from localized in vivo proton NMR spectra. Magn Reson Med 1993;30:672–9. doi:

10.1002/mrm.1910300604.

24 Wilson M, Andronesi O, Barker PB, et al. Methodological consensus on clinical proton MRS of the brain: review and recommendations. Magn Reson Med 2019;82:527–50. doi: 10.1002/mrm.27742.

25 Zhou M, Zhou Y, Liao H, et al. Diagnostic accuracy of 2-hydroxyglutarate magnetic resonance spectroscopy in newly diagnosed brain mass and suspected recurrent gliomas. Neuro-Oncology 2018;20:1262–71. doi: 10.1093/neuonc/noy022.

26 Fischl B, Salat DH, Busa E, et al. Whole brain segmentation: automated labeling of neuroanatomical structures in the human brain. Neuron 2002;33:341–55. doi: 10.1016/s0896-6273(02)00569-x.

27 Greve DN, Salat DH, Bowen SL, et al. Different partial volume correction methods lead to different conclusions: an (18)F-FDG-PET study of aging. Neuroimage 2016;132:334–43. doi: 10.1016/j.neuroimage.2016.02.042.

28 Matsuoka K, Takado Y, Tagai K, et al. Two pathways differentially linking tau depositions, oxidative stress, and neuronal loss to apathetic phenotypes in progressive supranuclear palsy. J Neurol Sci 2023;444:120514. doi: 10.1016/j.jns.2022.120514.

29 Gozdas E, Hinkley L, Fingerhut H, et al.. 1H-MRS neurometabolites and associations with neurite microstructures and cognitive functions in amnestic mild cognitive impairment. NeuroImage Clin 2022;36:103159. doi: 10.1016/j.nicl.2022.103159.

30 Tumati S, Opmeer EM, Marsman JC, et al. Lower choline and myo-inositol in temporo-parietal cortex is associated with apathy in amnestic MCI. Front Aging Neurosci 2018;10:106. doi: 10.3389/fnagi.2018.00106.

31 Strom A, Iaccarino L, Edwards L, et al. Cortical hypometabolism reflects local atrophy and tau pathology in symptomatic Alzheimer's disease. Brain 2022;145:713–28. doi: 10.1093/brain/awab294.

32 Riederer I, Bohn KP, Preibisch C, et al. Alzheimer disease and mild cognitive impairment: integrated pulsed arterial spin-labeling MRI and (18)F-FDG PET. Radiology 2018;288:198–206. doi: 10.1148/radiol.2018170575.

33 Pradhan S, Bonekamp S, Gillen JS, et al. Comparison of single voxel brain MRS AT 3T and 7T using 32-channel head coils. Magn Reson Imaging 2015;33:1013–8. doi: 10.1016/j.mri.2015.06.003.

34 Li S, Cai Y, Liu J, et al. Dissociated roles of the parietal and frontal cortices in the scope and control of attention during visual working memory. Neuroimage

2017;149:210–19. doi: 10.1016/j.neuroimage.2017.01.061.

35 Owen AM, McMillan KM, Laird AR, et al. N-back working memory paradigm: a meta-analysis of normative functional neuroimaging studies. Hum Brain Mapp 2005;25:46–59. doi: 10.1002/hbm.20131.

36 Khalil M, Teunissen CE, Otto M, et al. Neurofilaments as biomarkers in neurological disorders. Nat Rev Neurol 2018;14:577–89. doi: 10.1038/s41582-018-0058-z.

FIGURE LEGENDS

Figure 1. Multiple voxels of interest VOIs and representative spectrum of MRSI.

a) We placed the multi-voxel VOIs at the level of the cingulate gyrus (yellow box). We obtained usable spectra from the 10 × 10 × 15 mm^3 voxels (green squares) within the PRESS excitation volume (white box). b) An example of spectral data, spectral fit, fit residual, baseline, and individual metabolite fits obtained from the voxel (blue voxel). Glu, glutamate; NAA, N-acetylaspartate; NAA, N-acetylaspartate; NAAG, N–acetyl–aspartyl–glutamate; MRSI, magnetic resonance spectrum imaging; PRESS, point-resolved spectroscopy; VOI, volume of interest.

Figure 2. Representative PET images and heatmaps of Z score means of ^{18}F-florzolotau and ^{11}C-PiB.

a, b) A representative PET image of ^{18}F-florzolotau (left) and ^{11}C-PiB (right) in patients with AD showed accumulations in the neocortical and limbic cortices. c, d) Z-score heatmaps of ^{18}F-florzolotau (left) and ^{11}C-PiB (right) in patients with AD also indicated marked increases in the neocortical and limbic cortices. AD, Alzheimer's disease; PET, positron emission tomography; PiB, Pittsburgh compound-B.

Figure 3. Heatmaps of Z score means of Glu/tCr and tNAA/tCr ratios and Pearson correlation coefficients with ^{18}F-florzolotau and ^{11}C-PiB SUVRs.

a, b) The heatmap showed decreased Z scores of Glu (upper) and tNAA (lower) to tCr ratio in the GM, especially in the PCC and right DLPFC in patients with AD. c, d) The heatmaps of Pearson correlation coefficients displayed a marked negative correlation of Glu/tCr ratios with ^{18}F-florzolotau SUVR in the PCC regions (upper), not but with ^{11}C-PiB (lower) in patients with AD. e, f) The heatmaps of Pearson correlation coefficients indicated no extensive areas where ^{11}C-PiB SUVRs were correlated with Glu (upper) and (lower) to the tCr ratio in patients with AD. Stars indicate that the absolute value of Pearson correlation coefficients is greater than 0.5. AD, Alzheimer's disease; Cr, creatine; DLPFC, dorsolateral prefrontal cortex; Glu, glutamate; GM, gray matter; NAA, N-acetylaspartate; PCC, posterior cingulate cortex; PET, positron emission tomography; PiB, Pittsburgh compound-B.

Figure 4. A representative image of combined voxels covering the PCC and right DLPFC and scatterplots showing differences in the Glu/tCr and tNAA/tCr ratios between the patients with AD and HCs.

a) A representative image of the combined voxels covering the PCC and right DLPFC.

b-e) Both the Glu/tCr and tNAA/tCr ratios were significantly decreased in the PCC and right DLPFC in patients with AD compared with those in the HCs (right upper, Glu/tCr ratios in the PCC; left upper, Glu/tCr ratios in the right DLPFC; right lower, tNAA/tCr ratios in the PCC; left lower, tNAA/tCr ratios in the right DLPFC). AD, Alzheimer's disease; Cr, creatine; DLPFC, dorsolateral prefrontal cortex; Glu, glutamate; HC, healthy control; NAA, N-acetylaspartate; PCC, posterior cingulate cortex; PET, positron emission tomography; PiB, Pittsburgh compound-B. * P values are <0.05, *** P values are <0.005, **** P values are <0.001.

Figure 5. Scatterplot showing correlations of Glu/tCr and tNAA/tCr ratios with ^{18}F-florzolotau SUVR in patients with AD.
We found a negative correlation between ^{18}F-florzolotau SUVRs and Glu/tCr ratios (left) in the PCC, but not with tNAA (right). AD, Alzheimer's disease; Cr, creatine; Glu, glutamate; NAA, N-acetylaspartate; PCC, posterior cingulate cortex.

Figure 6. Scatterplot showing correlations of Glu/tCr and tNAA/tCr ratios with cognitive batteries in patients with AD.
a, b) The Glu (upper left) and tNAA/tCr ratios (upper right) in the DLPFC were positively correlated with MMSE total scores in patients with AD. c, d) We also found a negative correlations between Glu/tCr ratios in the PCC and TMT-A time (lower left) and between tNAA/tCr ratios in the right DLPFC and TMT-B time (lower right) in patients with AD. AD, Alzheimer's disease; Cr, creatine; DLPFC, dorsolateral prefrontal cortex; Glu, glutamate; NAA, N-acetylaspartate; PCC, posterior cingulate cortex.

Figure 7. Scatterplots showing the comparison of blood NfL levels and the correlations of Glu/tCr and tNAA/tCr ratios with blood NfL levels in patients with AD.
a) We found higher NfL levels in the blood of patients with AD than that in HCs. b-e) We found significant negative correlations between blood NfL levels and Glu/tCr ratios (upper right) and tNAA/tCr ratios (lower right) in the right DLPFC. There were also negative correlations between blood NfL levels and Glu/tCr ratios (upper left) and tNAA/tCr ratios (lower left) in the PCC, although these correlations did not reach a statistical significance level. AD, Alzheimer's disease; Cr, creatine; DLPFC, dorsolateral prefrontal cortex; Glu, glutamate; NAA, N-acetylaspartate; NfL, neurofilament light chain; PCC, posterior cingulate cortex. *** P values are <0.005.

Table 1. Demographic characteristics

	AD (n = 19)	HC (n = 26)		
	Mean (SD) or frequency (%)	Mean (SD) or frequency (%)	t or χ^2	P
Sex			$\chi^2 = 0.77$	0.28
Female	12 (63.2)	13 (50)		
Male	7 (36.8)	13 (50)		
Age, years	67.8 (9.4)	67.8 (7.5)	$t = -0.007$	0.99
Education, years	14.1 (1.9)	14.7 (1.5)	$t = -1.15$	0.26
MMSE	22.1 (4.0)	28.8 (1.3)	$t = -7.14$	<0.001
TMT-A time [a]	69.9 (31.5)	35.5 (9.2)	$t = 4.50$	<0.001
TMT-B time [b]	197.0 (93.6)	85.4 (32.0)	$t = 4.47$	<0.001
GDS	3.4 (2.2)	2.9 (2.8)	$t = 0.65$	0.52
Apathy Scale	13.5 (5.2)	10.9 (7.5)	$t = 1.32$	0.19
CDR global score		N/A	N/A	N/A
0.5	8 (42.1)			
1	9 (47.4)			
2	2 (10.5)			

Note: AD, Alzheimer's disease; CDR, clinical dementa rating; GDS, geriatric depression scale; HC, healthy control; MMSE, mini-mental state examination; SD, standard deviation.

[a] We presented available TMT-A data of 18 patients with AD/MCI and 26 HC participants.

[b] We presented available TMT-B data of 15 patients with AD/MCI and 26 HC participants.

a)

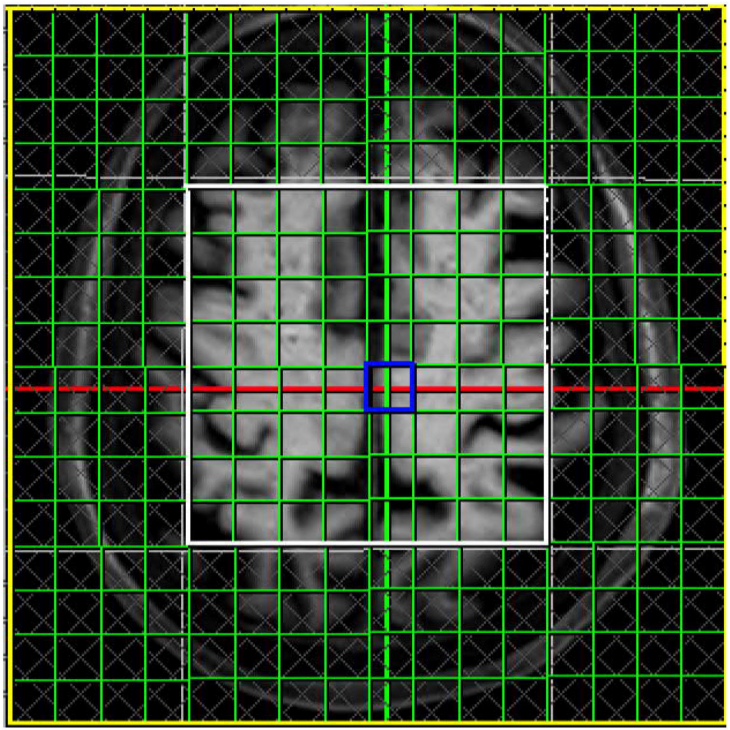

b)

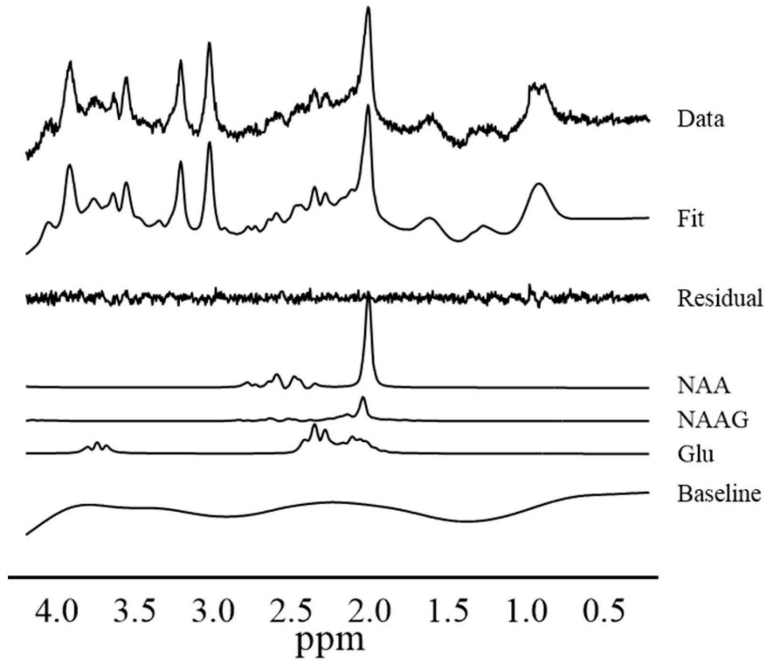
Data
Fit
Residual
NAA
NAAG
Glu
Baseline
4.0
3.5
3.0
2.5
2.0
1.5
1.0
0.5
ppm

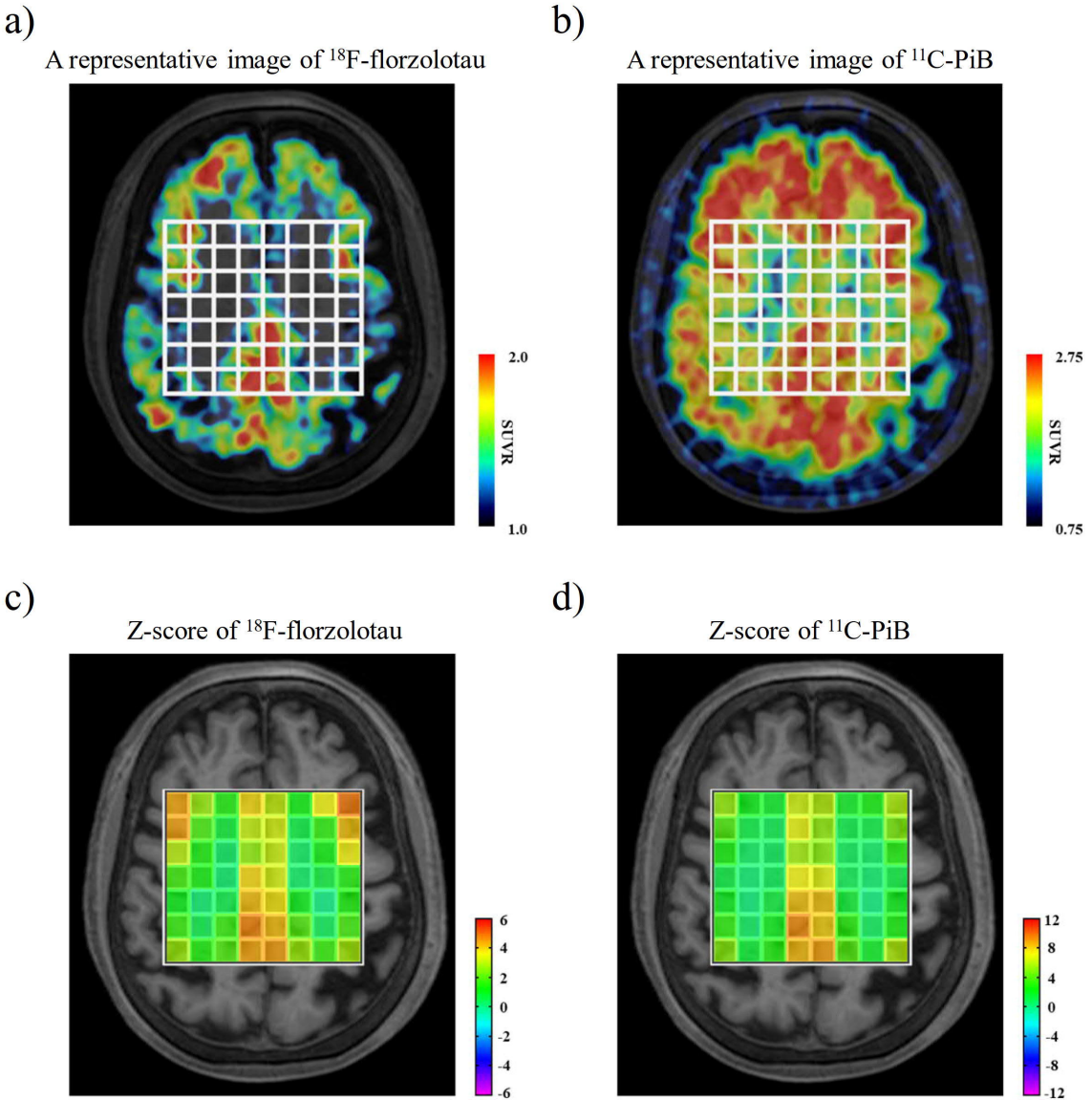
a)
A representative image of 18F-florzolotau
2.0
SUVR
1.0
b)
A representative image of 11C-PiB
2.75
SUVR
0.75
c)
Z-score of 18F-florzolotau
6
4
2
0
-2
-4
-6
d)
Z-score of 11C-PiB
12
8
4
0
-4
-8
-12

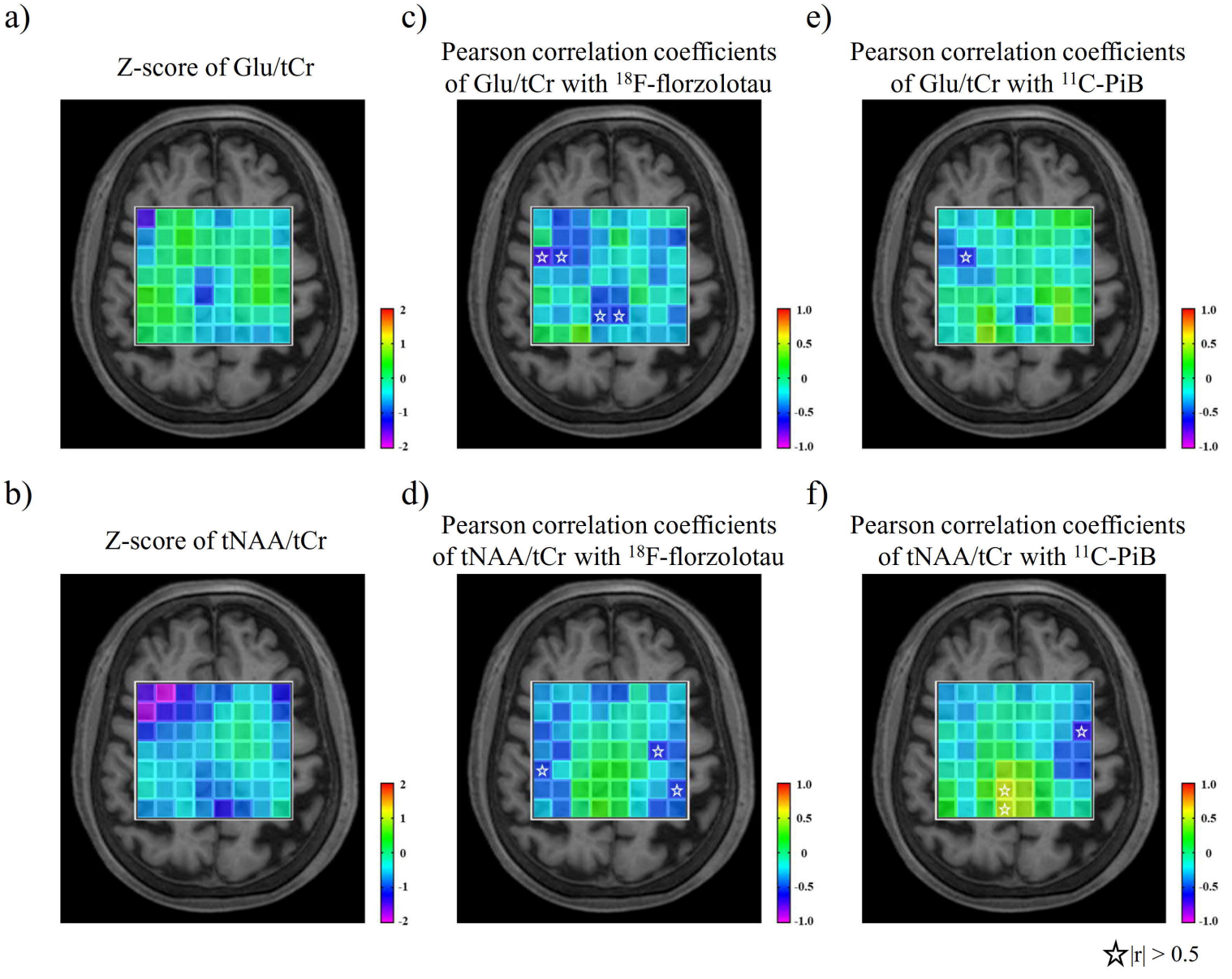
a)
Z-score of Glu/tCr
2
1
0
-1
-2
b)
Z-score of tNAA/tCr
2
1
0
-1
-2
c)
Pearson correlation coefficients of Glu/tCr with 18F-florzolotau
1.0
0.5
0
-0.5
-1.0
d)
Pearson correlation coefficients of tNAA/tCr with 18F-florzolotau
1.0
0.5
0
-0.5
-1.0
e)
Pearson correlation coefficients of Glu/tCr with 11C-PiB
1.0
0.5
0
-0.5
-1.0
f)
Pearson correlation coefficients of tNAA/tCr with 11C-PiB
1.0
0.5
0
-0.5
-1.0
☆|r| > 0.5

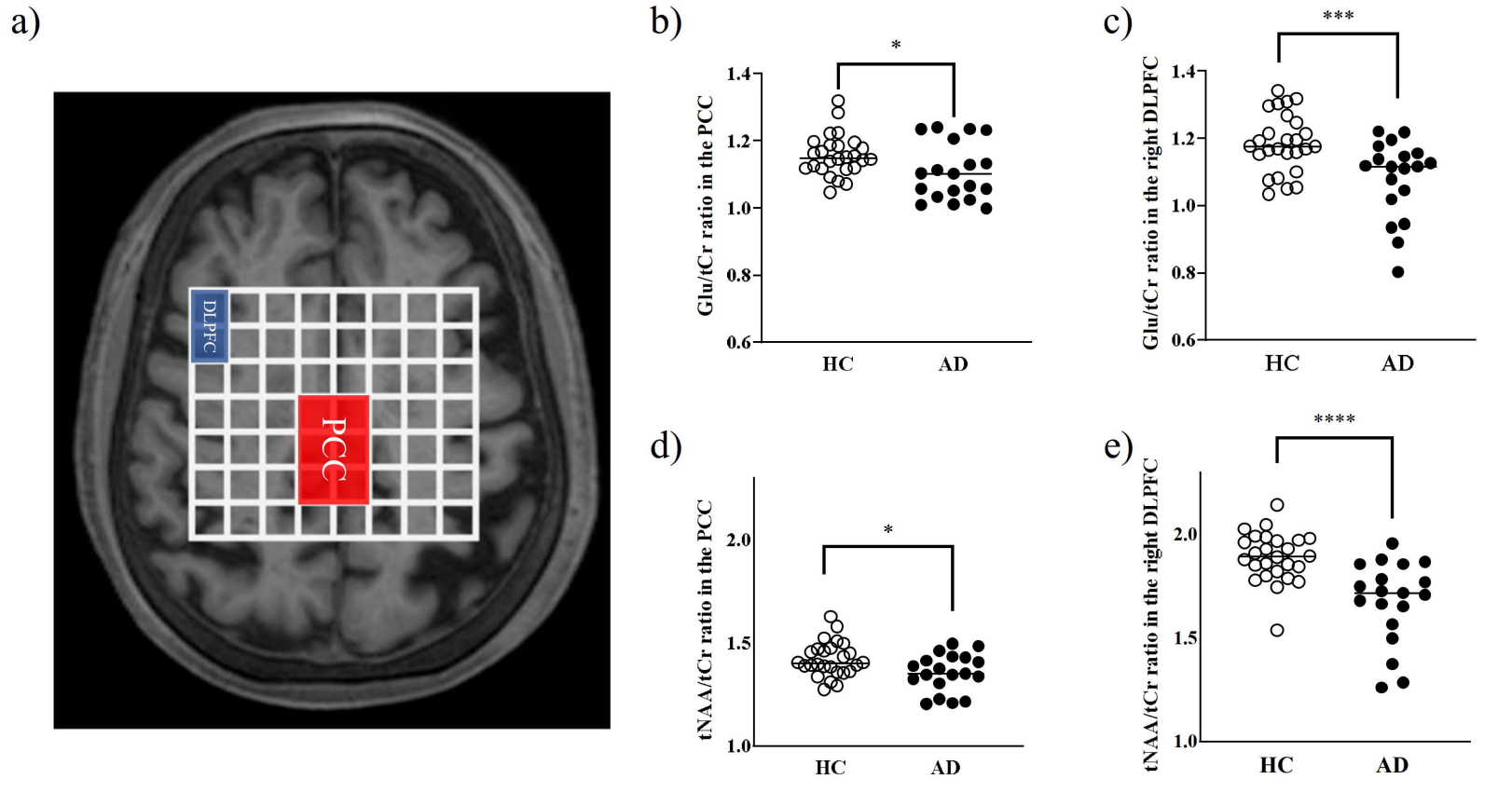
a)
DLPFC
PCC
b)
*
Glu/tCr ratio in the PCC
1.4
1.2
1.0
0.8
0.6
HC
AD
c)
***
Glu/tCr ratio in the right DLPFC
1.4
1.2
1.0
0.8
0.6
HC
AD
d)
*
tNAA/tCr ratio in the PCC
2.0
1.5
1.0
HC
AD
e)
****
tNAA/tCr ratio in the right DLPFC
2.0
1.5
1.0
HC
AD

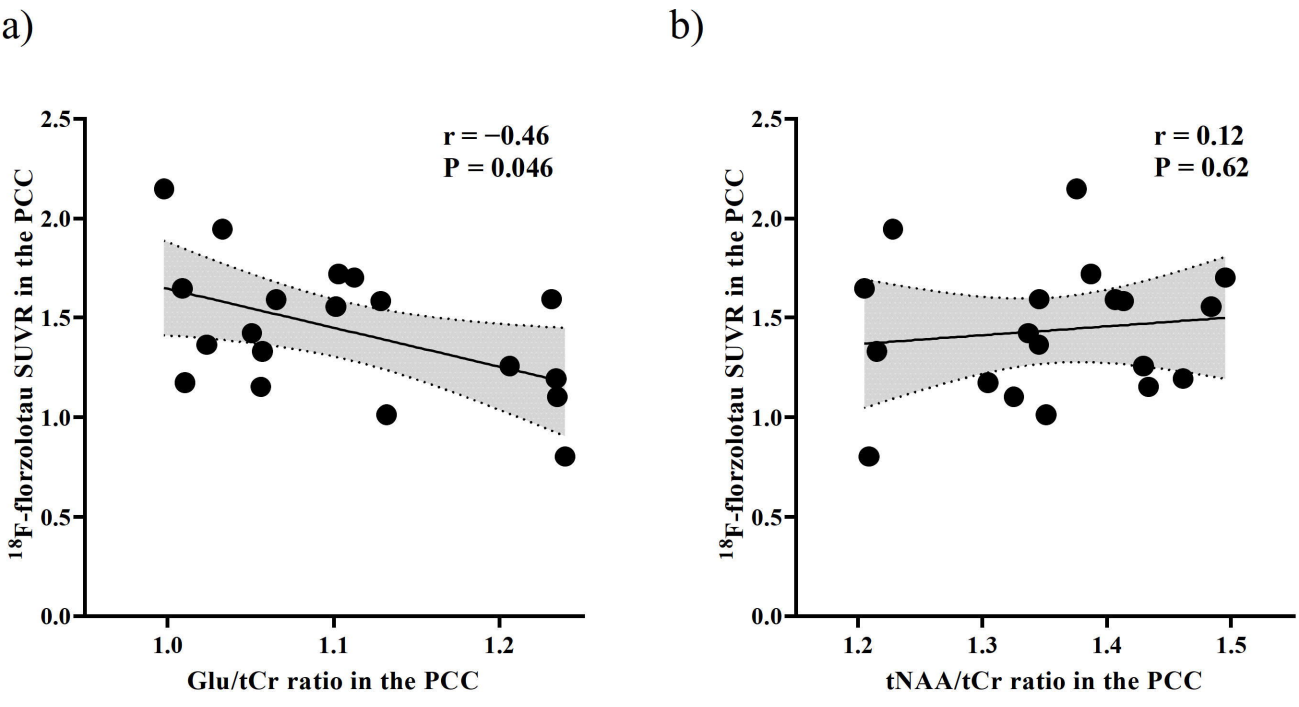
a)
r = −0.46
P = 0.046
18F-florzolotau SUVR in the PCC
Glu/tCr ratio in the PCC
0.0
0.5
1.0
1.5
2.0
2.5
1.0
1.1
1.2
b)
r = 0.12
P = 0.62
18F-florzolotau SUVR in the PCC
tNAA/tCr ratio in the PCC
0.0
0.5
1.0
1.5
2.0
2.5
1.2
1.3
1.4
1.5

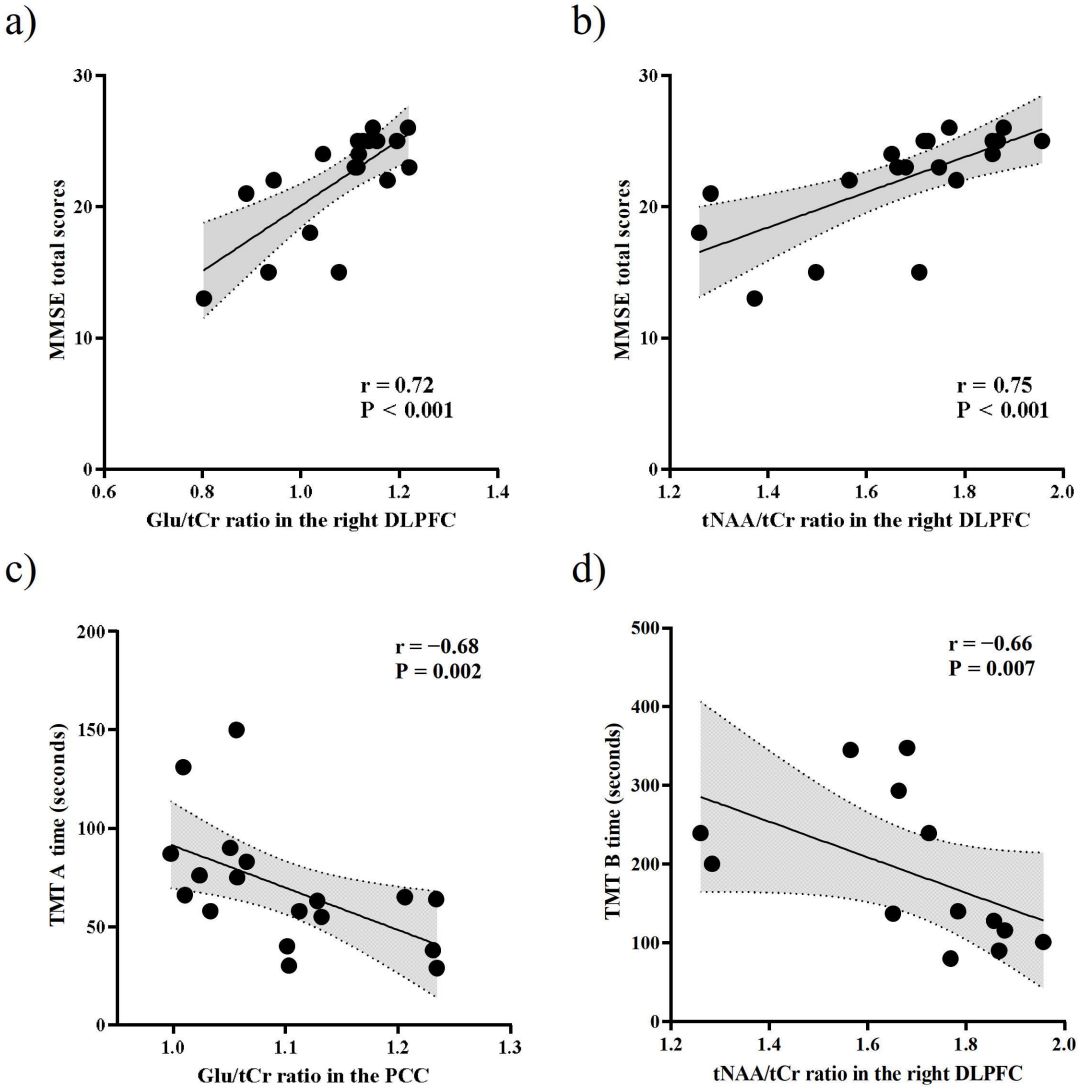
a)
MMSE total scores
Glu/tCr ratio in the right DLPFC
r = 0.72
P < 0.001
b)
MMSE total scores
tNAA/tCr ratio in the right DLPFC
r = 0.75
P < 0.001
c)
TMT A time (seconds)
Glu/tCr ratio in the PCC
r = −0.68
P = 0.002
d)
TMT B time (seconds)
tNAA/tCr ratio in the right DLPFC
r = −0.66
P = 0.007

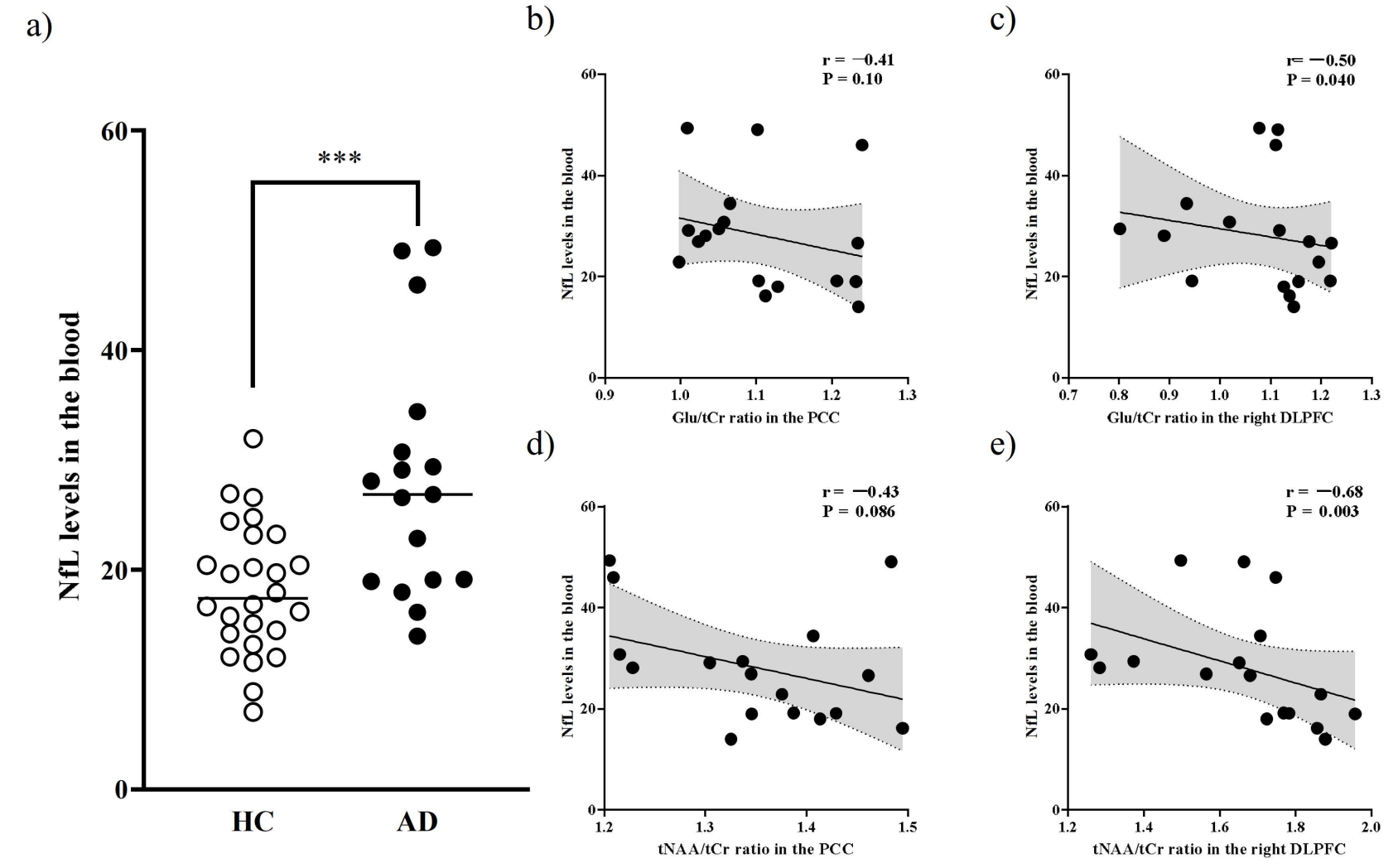
a)
***
NfL levels in the blood
60
40
20
0
HC
AD
b)
r = −0.41
P = 0.10
NfL levels in the blood
Glu/tCr ratio in the PCC
c)
r= −0.50
P = 0.040
NfL levels in the blood
Glu/tCr ratio in the right DLPFC
d)
r = −0.43
P = 0.086
NfL levels in the blood
tNAA/tCr ratio in the PCC
e)
r = −0.68
P = 0.003
NfL levels in the blood
tNAA/tCr ratio in the right DLPFC